2018 IEEE-RAS 18th International Conference on Humanoid Robots (Humanoids)
Beijing, China, November 6-9, 2018

Online Rolling Motion Generation for Humanoid Falls Based on Active Energy Control Concepts

Rajesh Subburaman, Nikos G. Tsagarakis, and Jinoh Lee

Abstract— **This paper introduces a novel online rolling over control technique based on energy concepts to alleviate impact forces during humanoid fall overs. To generate efficient rolling motion, critical parameters are defined by the insights drawn from a study on rolling, which are contact positions and attack angles. In addition, energy-injection velocity is proposed as an auxiliary control command to ensure sequential multiple contacts in rolling. The online rolling controller is synthesized to compute the optimal values of three rolling parameters: the first two parameters are to construct the humanoid's posture as a polyhedron by selecting suitable contacts points. This polyhedron distributes the energy gradually across multiple contacts; and the last one is to inject additional energy into the system during the fall, to overcome energy drought and tip over successive contacts, i.e., rolling. Accordingly, the proposed controller exploits energy injection, minimization, and distribution techniques and renders a rolling like motion. Numerical experiments with a segmented planar model and a full humanoid model verify that it significantly reduces impact forces.**

I. Introduction

Biped humanoids due to their structure have several advantages over other robots to operate in unstructured environments designed for humans. In such situations, falling over is inevitable for humanoids and to operate continuously they should sustain minimal damages and recover autonomously. This has prompted the researchers to address issues such as fall prediction [1], controlled fall [2], and recovery from it [3]. This paper in particular focuses on the controlled fall problem.

In the past two decades, several works reported different controlled fall techniques to reduce the impact forces. Fujiwara et *al.* proposed a preplanned motion sequence inspired by Ukemi in [2] which was extended further with optimal control to generate safe falling motions in [4], [5]. In addition, the authors in [6]–[10] presented controlled fall techniques with different combinations of inertia/posture reshape, auxiliary devices, external passive and internal active compliances. There are also other works, wherein, recorded human falling motions were either used to design controllers using cost functions as in [11], or extract motion primitives such as knee/hip bending accompanied by stretching to devise motion strategies for falling humanoids [12]. However, because the aforementioned works are either system or direction specific, and some required careful design of motion sequences and postures, they are less adaptable to handle generic falls.

This work is supported by the European Community's H020 robotics program ICT-23-2014, grant agreement 644727—CogIMon.

The authors are with Department of Advanced Robotics, Istituto Italiano di Tecnologia (IIT), Via Morego 30, 16163, Genova, Italy.

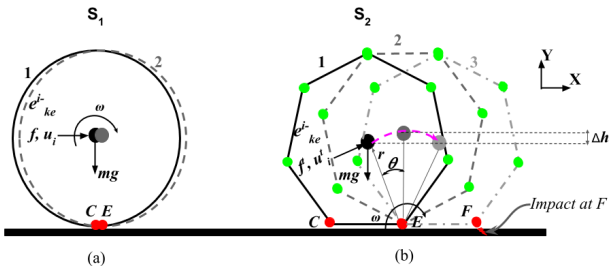

Fig. 1. Dynamics involved in the rolling of two systems: (a) circle and (b) polygon (heptagon).

The above drawbacks gave rise to several optimization and learning based controllers lately, with an attempt to automate the generation of controlled fall motion. Notable works include reinforcement based optimal location of hand contact to reduce energy conversion [13], Markov decision process based multi-contact planning [14], a parametric model for falling motion using policy gradient reinforcement learning [15] and actor-critic neural network to select simultaneously the contact body, its location, time and corresponding joint torques [16]. The above works addressed mainly sagittal falls, in particular, forward falls, and most of them require training over a significant number of trials. These requirements limit their chances to apply online and handle different direction falls.

To address the above limitations, we propose a rolling motion generation controller to handle humanoid fall overs. Since the generated motion is multi-contact, we hypothesize it to reduce the impact forces considerably. The proposed controller is inspired by Ukemi, like in [2], [4], [5]. Whereas, this is different owing to the following novel contributions: 1) online rolling controller (ORC) to compute the sub-optimal contact poses and to regulate the system's energy, 2) energy-based control actions, and 3) notion of energy distribution polyhedron (EDPH) to realize the sub-optimal rolling posture.

In reference to the rolling motion, there is a unique work which involves the generation of rolling for humanoids associated with the controlled fall reported in [14]. In this work the authors generate a multi-contact motion for a falling humanoid using dynamic programming. However, it requires offline training and optimization, and is limited to sagittal falls. On the other hand, the proposed method can be applied online, and handle both sagittal and frontal falls. Henceforth, this is the first instance that an online controller addressing rolling to reduce the impact forces during the humanoid fall

overs has been reported. Regarding energy-based methods, only few works have been reported in the controlled fall of humanoids. In [13], the authors propose a control strategy inspired by energy conversions, however, it is not actively used to generated control actions. In the authors' previous work [17], the energy has been considered actively in not only devising the fall strategy but also generating control actions. Whereas, we have additionally explored energy injection and rolling motion in this paper.

II. Insights on Rolling

A. Why Rolling is important for Controlled Fall?

Most of the present controlled fall techniques generate motions which involve less number of body/ground contacts. Though the resulting motions have been reported to reduce the impact forces, they are less dynamic, unlike the Ukemi motion. The discrepancy is mainly due to the less number of contacts and arbitrary body postures observed with the present controlled fall techniques. One can notice that martial arts professional, who perform Ukemi motion, maintain continuous contact with the ground during fall by shaping their body (primarily using their arms and torso) in the form of a sphere/circle and roll over their shoulders. This motion avoids damage to their vital parts such as the head and hip. The basic principle is to make continuous contacts with the ground to gradually dissipate the accumulated kinetic energy, resulting in a rolling motion. While humans have muscles and compliant joints to absorb the impact during their fall over, they are still prone to major damages without a breakfall technique such as Ukemi. Hence, we believe that Ukemi like rolling is paramount to reduce the impact forces significantly during the fall over of humanoids. Unlike humans, humanoids being rigid, the above motion can be realized by constructing a polyhedron (i.e., convex hull) with the potential contacts selected around its body. The construction of the polyhedron will be discussed elaborately in Section V.

B. How does Energy Affect Rolling?

In order to generate a rolling motion with a polyhedron, it is necessary to understand how a system's energy influences its motion. For simplicity, a planar example is considered for illustration as shown in Fig. 1. It includes two planar point mass (m) systems, a circle (S_1) and a heptagon (S_2). Here, S_2 is used to represent the rolling motion of a humanoid in 2D. Let $\mathbf{u}_i$, $\mathbf{f}$, ω, $g = 9.8m/s^2$, and e_{ke}^{i-} represent initial velocity, force acting on the system, angular velocity of rolling/tipping, acceleration due to gravity, and initial kinetic energy of the system respectively. Assuming energy loss due to friction is less, S_1 with e_{ke}^{i-} can make continuous rolling contacts such as C, E, ... with minimal loss of energy. However, for S_2 with e_{ke}^{i-}, it can only tip over E, if it satisfies the following *energy rolling condition*:

$$e_{\text{ke}}^{i-} \geq w_{\text{E}}, \tag{1}$$

where $w_{\text{E}} = \mathrm{f}^{\mathrm{t}} \cdot r\theta$ is the work to be done by S_2 against g to move for an arc length of $r\theta$ to reach the state 2, and f^{t} is the tangential force to the arc. For consecutive tip overs to be successful, the above condition should be satisfied. Further, because the consecutive rolling contacts made with S_2 is more discontinuous when compared to S_1, the energy is lost in the form of heat or deformation due to the impact at each contact. For instance, Fig. 1b shows the tipping over motion from the state 2 to 3, resulting in an impact at F. Such impacts can reduce the energy considerably leading to the violation of energy rolling condition, and this may halt the system abruptly. Interestingly, the above condition can be avoided by injecting additional energy into the system, more of which is discussed in Section IV-C.

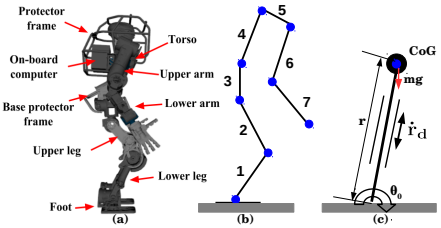

Fig. 2. Different representation of a humanoid robot model, WALK-MAN [18] considered here for instance: (a) Complete numerical model of the robot, (b) Segmented planar robot model (SPR), and (c) Telescopic inverted pendulum model (TIP).

III. Rolling Problem

In this section, we discuss what is required to realize the rolling motion with falling over humanoids, and the necessary models to do so. The insights which we made in Section II such as the significance of rolling in reference to humanoids fall over, the influence energy has on rolling, and the condition to be maintained for successive contacts are actively used here.

1) Models and Critical Rolling Parameters: As stated earlier, energy influences rolling, and for it to be efficient, the dissipation of energy should be distributed across all the contacts. This can be attained by carefully choosing the key parameters: contact location and its attack angles. It is important to compute these parameters since they strongly determine the performance of rolling which in turn depends on the robot posture. In this paper we employ two different models of the full humanoid robot as shown in Fig. 2. Figure 2b denotes a relatively less complex segmented planar robot (SPR) model with 7 links. Links 1-7 represent the foot and lower-, upper-leg, waist, torso, torso-shoulder connector, upper-, and lower-arm, respectively. Figure 2c shows the simple telescopic inverted pendulum model (TIP), where m, r, $\dot{r}_d$, and θ_0 denote the point mass, length, sliding velocity and tipping angle.

2) How to choose the parameter values?: Ideally, for a fixed e_{ke}^{i-}, the parameters have to be chosen in such a way that apart from satisfying (1), the work done by the system at each contact should be more or less equal. The influence of the parameters on rolling is explained analytically with the SPR model as shown in Fig. 3. In the figure, the blue circle represents the CoG of the robot, the dotted circle denotes its projection on different links, and $cg_{\text{x}\bullet}$ and $cg_{\text{y}\bullet}$

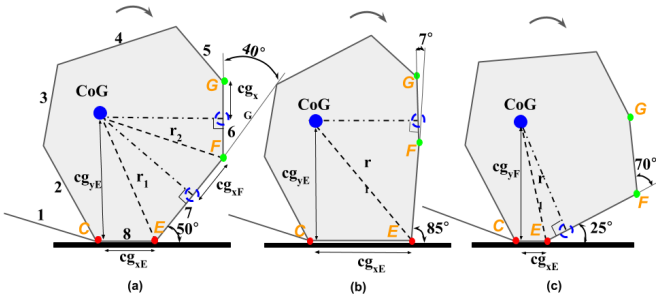

Fig. 3. SPR in three different configurations, assuming C as its primary contact (a)$\theta_{\text{att1}} \approx 50°$, (b)$\theta_{\text{att1}} = 85°$ and (c)$\theta_{\text{att1}} = 25°$.

are its relative x and y coordinates from the contact •. The robot here is assumed to have made primary contact with C, and it is about to make its secondary contact with E. Here, the contact locations E, F, and G; the attack angles $\theta_{\text{att1}} = \pi - \angle\text{CEG}$, and $\theta_{\text{att2}} = \pi - \angle\text{EFG}$ are the parameters that need to be determined to roll over the selected contacts. Setting a high value (e.g., 85°) for θ_{att1} as shown in Fig. 3b reduces the convexity of the polygon (becomes a straight line) and also increases cg_{xE}. While the former can result in unequal distribution of energy due to a non-smooth transition of contacts, the latter can reduce the chances of tipping over E (high w_{E}). Similarly, too small value (e.g., 25°) shown in Fig. 3c can increase the convexity of the polygon. But the projection of CoG on link 7 (cg_{xF}) after tipping over E is far away to considerably reduce the chances to roll over F (high w_{F}). However, by setting an intermediate value we observe that E is closer to CoG, also $cg_{\text{xF}} \approx 0.5||\mathbf{p}_{\text{EF}}||_2$ and $cg_{\text{xG}} \approx 0.5||\mathbf{p}_{\text{FG}}||_2$ ensures the closeness of CoG to successive contacts F and G, which in turn increases the chances of rolling over the selected contacts.

IV. Online Rolling Controller

The optimal values for the aforementioned parameters are computed online using the controller proposed here. After predicting the inevitable fall instance of a humanoid, its state is given as input to the controller, which in turn uses the TIP and SPR models to compute the optimal values of the parameters. The controller processes are shown in Fig. 4 and explained briefly in the following subsections.

A. State Estimation at the instant of Primary Contact

Since we intend to carry out the rolling motion after making primary contact with C, it is necessary to determine the state of the robot, i.e., velocity ($\mathbf{v}_{\text{C}}^-$), acceleration ($\mathbf{a}_{\text{C}}^-$) and CoG ($\mathbf{cg}$) just before making the contact. The TIP and SPR models are used here to determine the state of the robot. The dynamics of the TIP model can be written as follows:

$$\dot{\mathbf{x}} = \mathcal{F}(\mathbf{x}, u) := \begin{bmatrix} (g\sin\theta_0 - 2\dot{r}\dot{\theta}_0)/r & \dot{\theta}_0 & u \end{bmatrix}^T, \quad (2)$$

where the state is defined as $\mathbf{x} = [\dot{\theta}_0\, \theta_0\, r]$, and r, θ_0, and u represent the pendulum length, tipping angle, and control input, respectively. Note that $u = \dot{r}_{\text{d}}$, where $\dot{r}_{\text{d}}$ is the desired sliding velocity determined by the energy shaping controller devised in [17]. This controller minimizes the total energy by

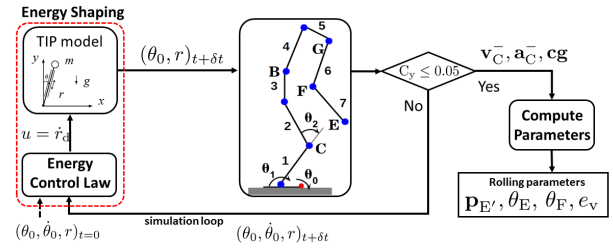

Fig. 4. The proposed Online Rolling Controller: taking the fall prediction state $(\theta_0, \dot{\theta}_0, r)$ as input and computing the parameters $\mathbf{p}_{\text{E}'}, \theta_{\text{E}}, \theta_{\text{F}}$, and e_{v}.

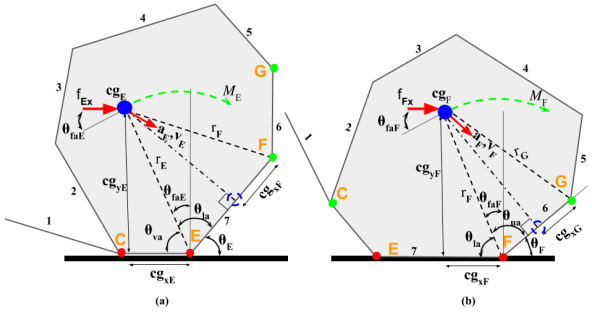

Fig. 5. SPR represented in the form of a polygon: (a) Position and the attack angle (θ_{E}) of E with the robot state v_{E} and a_{E}), and (b) those of F with the robot state v_{F} and a_{F}.

lowering the robot's CoG (crouching action), which results in the primary contact C.

Given a disturbance to the robot and upon predicting its fall, TIP model is simulated with the energy shaping control law to determine at each time step θ_0 and r as shown in Fig. 4. This is then sent to the SPR model to compute the new joint position of the ankle (θ_1) using inverse kinematics as,

$$\theta_1 = \sin^{-1}((\text{C}_{des} - l_0\sin(\theta_0))/l_1), \quad (3)$$

where $\text{C}_{\text{des}} = \text{C}_{\text{y,ini}} + (r_{\text{ini}} - r)/2$ denotes the desired height of the knee, r_{ini} and $\text{C}_{\text{y,ini}}$ are the initial pendulum length and knee height respectively. With θ_0 and θ_1, the new knee height (C_{y}) can be given as

$$\text{C}_y = l_0\sin(\theta_0) + l_1\sin(\theta_1 + \theta_0). \quad (4)$$

The above sequence is repeated until $\text{C}_{\text{y}} \le 0.05m$ (knee touch down). With the above condition satisfied, the tangential velocity $(v_{\text{C}}^-)_t = r\dot{\theta}_0$ and acceleration $(a_{\text{C}}^-)_t = r\ddot{\theta}_0 + \dot{r}\dot{\theta}_0$ can be computed. With $(v_{\text{C}}^-)_t$, $(a_{\text{C}}^-)_t$, r, and θ_0 the state of the robot can be determined as

$$\mathbf{v}_{\text{C}}^- = v_{\text{C}}\cdot\mathbf{k},\ \mathbf{a}_{\text{C}}^- = a_{\text{C}}\cdot\mathbf{k},\ \mathbf{cg} = r_{\text{C}}\cdot\mathbf{k},\ \mathbf{k} := [\sin\theta_0\ \ \cos\theta_0]. \quad (5)$$

B. Critical Rolling Parameters (CRP)

1) Optimal contact position: In order to achieve a smooth rolling motion, it is necessary to maintain continuous contact with the ground. With C being the primary contact, E is chosen as the secondary contact due to its proximity to the ground. To prevent further conversion of the robot's potential energy (PE) to kinetic energy (KE) the z coordinate of E is maintained at the same level of C, leaving only the x coordinate of E (E_{x}) to be determined as shown in Fig. 5a.

As discussed in Section II-A, E_x can neither be too close nor too far, hence its optimal location can be computed by equating the moment w.r.t. E and solving for cg_{xE} as

$$cg_{xE} = (f_{Ex} \cdot cg_{yE})/m \cdot g. \tag{6}$$

where f_{Ex} is the x component force acting on the system after contact E (assuming E and C contacts are made simultaneously). From cg_{xE}, the optimal value of E_x is determined as $E_x = cg_x + cg_{xE}$. Since the state of the system changes immediately after the contact due to the impact with the ground, the new state at contact E can be computed as follows:

$$(v_E^+)_t = \sqrt{(e_{ke}^{E+} \cdot 2)/m}, \quad (a_E^+)_t = ((v_E^+)_t^2 - (v_E^-)_t^2)/2s, \tag{7}$$

where e_{ke}^{E+} and s denote the system's kinetic energy and it's rebound after contact E, respectively. They can be given as

$$e_{ke}^{E+} = \epsilon . e_{ke}^{E-}, \quad s = ((v_E^-)_t^2 - (v_E^+)_t^2)/2g. \tag{8}$$

where ϵ is the coefficient of restitution. For instance, if contacting parts of the robot are made of high strength aluminium alloy (7076), ϵ = 0.35 [19].

2) Computation of attack angles: The angle made by the contacts E (θ_E) and F (θ_F) are computed in this section as explained below. Since we intend a continuous rolling motion, in order to dissipate the energy gradually across the contacts, it is preferable to maintain the same tipping radius, i.e., r_E = r_F = r_G. The tipping radius about contact E (r_E) can be computed from the position of E and CoG. With the length of the lower arm link $||\mathbf{p}_{EF}||$, and upper arm link $||\mathbf{p}_{FG}||$, θ_E and θ_F can be computed as

$$\theta_E = \cos^{-1}((0.5||\mathbf{p}_{EF}||)/r_E), \tag{9}$$

$$\theta_F = \cos^{-1}((0.5||\mathbf{p}_{FG}||)/r_F). \tag{10}$$

C. Energy Injection

A system's continuous rolling depends not only on its contact positions and attack angles but also on the *energy rolling condition* (1). Failing to satisfy (1) could hamper the rolling motion of a system, called *energy drought*. The drawback of this is the reduction of the number of contacts over which initial kinetic energy e_{ke}^- is distributed, then, this relatively increases the impact force at the last contact. In this paper, we propose to avoid the energy drought condition by injecting energy into the system in the beginning of the rolling motion. The energy injection process is briefly explained below.

With the robot's state—$\mathbf{v}_E^-$, $\mathbf{a}_E^-$, and $\mathbf{cg}$—just before making the contact C/E known from simulating the TIP model, the initial kinetic energy can be computed as $e_{ke}^{E-} = 0.5m \cdot (v_E^-)^2$. The energy available after each impact for rolling over any contact point i can be computed as

$$e_{ke}^i = \epsilon \cdot e_{ke}^{i-}, \tag{11}$$

for example, at contact point E, $e_{ke}^{E+} = \epsilon \cdot e_{ke}^{E-}$. With the state after impact at E computed in (7), the work done in rotating the system over a radius r_E about E can be computed as

$$w_E = mgr_E(1 - \cos(\theta_{faE})), \tag{12}$$

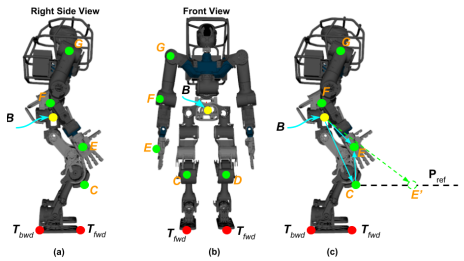

Fig. 6. Right (a) and front (b) side view of WALK-MAN with the potential contacts selected for right arm roll. (c) Position of E' along the primary reference line (P_{ref}) for the secondary contact E.

where the right side term denotes the change in system's potential energy during the tipping motion. Even though the total rotation of the system about E would be θ_E as shown in Fig 5a, only until θ_{faE} work is done by the system since it involves raising the CoG against the gravity, while for ($\theta_E - \theta_{faE}$) the work is done by the gravity due to the lowering of CoG. It is necessary to satisfy the condition, $e_{ke}^{E+} \geq w_E$, to successfully roll over E. Similarly, the *energy rolling condition* can be verified for other contacts.

With the available energy and the work done computed separately for each contact, the total work done and the total available energy can be computed as $w^t = w_E + w_F$ and $e_{ke}^t = e_{ke}^{E+} + e_{ke}^{F+}$. The energy to be injected at each contact ($e_{ke,inj}^i$) is computed as

$$e_{ke,inj}^i = \begin{cases} (w^i - e_{ke}^i)/\epsilon^i, & \text{if } w^i > e_{ke}^i \\ 0, & \text{otherwise.} \end{cases} \tag{13}$$

The total energy needs to be injected can be written as $e_{ke,inj}^t = \sum_{i=1}^n e_{ke,inj}^i$. Then, the injection velocity e_v is obtained as

$$e_v = \sqrt{(2 \cdot e_{ke,inj}^t)/m}. \tag{14}$$

By setting this to the system at the beginning of the controlled fall, we can realize continuous rolling motion without succumbing to *energy drought* condition.

V. Energy Distribution Polyhedron

In the previous section, the optimal values for the critical rolling parameters were computed using the TIP and SPR models. Those are used here to construct a polyhedron with the potential contacts selected around the humanoid's (WALK-MAN [18]) body to generate a rolling motion. The construction process is explained briefly below for the forward fall case.

The construction of EDPH involves three major steps: selection of potential contacts and determining the sub-optimal location for secondary contact, alignment of the contacts to ensure their successive touch down on the ground, and finally, orienting the set of contacts along the falling direction. The proposed forward rolling can be done on either arm, here the right arm is considered for the explanation, and Fig. 6 shows the potential contacts selected for it. C and D represent the left and right leg knee, and E, F, and G denote the right arm's hand, elbow, and shoulder contacts

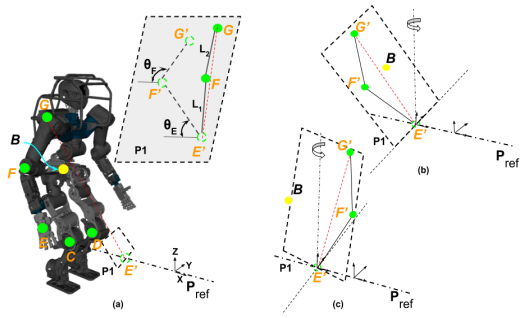

Fig. 7. (a) Potential contacts for right side forward fall with plane P1 and the alignment of the contacts $E^{'}$, $F^{'}$ and $G^{'}$. Initial (b) and final (c) orientation of P1 with the contacts aligned.

respectively. While T_{fwd} and T_{bwd} denote the forward and backward tipping point, and B represents the local base frame of the robot.

The knee contacts (C and D) are assumed to be the primary contacts due to the crouching action of energy shaping (ES). For the right shoulder roll (discussed here), the right knee contact C, in particular, is taken as a reference and the optimal location of E, i.e., E' is computed as stated in Section IV-B.1.

Following the contacts C and E', the other contacts (F and G) are aligned to ensure continuous successive touch down on the ground. This is done by first constructing a plane with E' and G, and then forming a convex polygon with E', F and G using the link lengths $L_1 = ||\mathbf{p}_{\text{EF}}||$ and $L_2 = ||\mathbf{p}_{\text{FG}}||$. The convexity of the polygon is controlled using the attack angles (θ_{E} and θ_{F}) computed with ORC in Section IV-B.2. Finally, the aligned contacts are oriented in the direction of the robot's fall by orienting the plane containing the contacts to the fall direction. The orientation is done with respect to the B frame. The initial and final orientation of the plane are shown in Figs. 7b and 7c respectively.

VI. Whole Body Control Scheme

The online whole body controller presented here to achieve the proposed rolling motion includes two major tasks, and they are executed in a hierarchical order as follows:

- Task 1: energy injection and shaping → CoG commands
- Task 2: energy distribution (rolling) → pose commands

The overview of the proposed controller is shown in Fig. 8. By predicting the inevitable fall of the robot using [20], the fall controller is triggered. While the ORC computes optimal values for CRP, Task 1 and Task 2 are performed with the default settings until an update is received from ORC. The following subsections explain briefly the details of each task.

A. Energy Injection and Shaping (EIS - Task 1)

This task is associated with minimizing the energy using energy shaping technique, as introduced in [17]. However, one addition here is the inclusion of e_{v} (in Section IV) to add some energy into the system to overcome *energy drought* during the multi-contact motion. The intended motion along with the energy shaping action is achieved by setting the desired velocity of CoG, $\dot{\mathbf{x}}_{\text{CoG}} = [e_{\text{vx}} + \dot{r}_{\text{d}} \cos(\theta_0)\ e_{\text{vy}}\ \dot{r}_{\text{d}} \sin(\theta_0)]$, where e_{vx} and e_{vy} represent the x and y components of e_{v} computed as $e_{\text{v}} \cos(\theta_{\text{dir}})$ and $e_{\text{v}} \sin(\theta_{\text{dir}})$. θ_{dir} represents the fall direction considered in Section V, and θ_0 is the tilting angle of the humanoid. The joint velocity reference ($\dot{\mathbf{q}}_{\text{T1}}$) for Task 1 can be computed as discussed in [17].

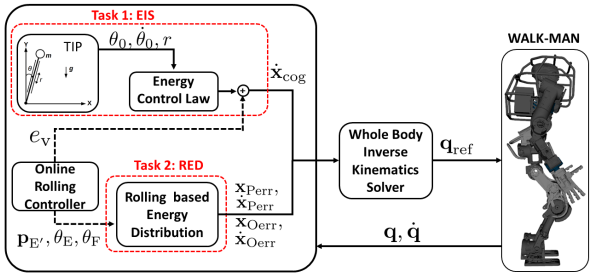

Fig. 8. Overview of the generalized online fall control for humanoids.

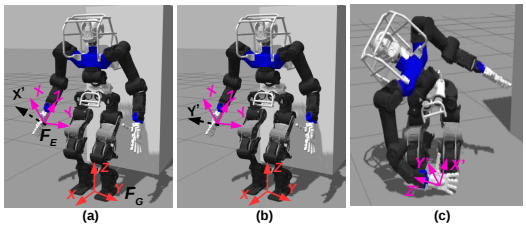

Fig. 9. Orientation control of the hand frame F_{E} with desired axes X', Y'

B. Rolling based Energy Distribution (RED - Task 2)

The EDPH discussed in Section V is used to distribute the minimized energy over multiple contacts, to result in a smooth rolling like motion. This is done by selecting suitable contacts over the robot's body, and controlling them to their respective optimal location ($\mathbf{x}_{\text{ref}}$) computed using the ORC. For forward falls, these contacts are primarily distributed over either left- or right-arm and the legs as shown in Fig. 6. In addition, to safeguard the hands during rolling motion, the X-axis of the wrist frame (F_{E}) is aligned to the global frame (F_{G}) as shown in Fig. 9. Further, in order to place the hand in a favorable position during rolling, the X and Y axes of F_{E} is oriented to X' and Y' axes respectively. The orientation of X' and Y' are determined based on θ_{E} and θ_{ort} obtained from Section V.

The desired joint velocities for Task 2 ($\dot{\mathbf{q}}_{\text{T2}}$) with the orientation control, can be written as

$$\dot{\mathbf{q}}_{\text{T2}} = \mathbf{N}_1 \mathbf{J}_{\text{con}}^{+} \left(\mathbf{K}_{\text{p}} \begin{bmatrix} \mathbf{x}_{\text{Perr}} & \mathbf{x}_{\text{Oerr}} \end{bmatrix}^T + \mathbf{K}_{\text{d}} \begin{bmatrix} \dot{\mathbf{x}}_{\text{Perr}} & \dot{\mathbf{x}}_{\text{Oerr}} \end{bmatrix}^T \right), \tag{15}$$

where $\mathbf{N}_1 \in \mathbb{R}^{\text{n}\times\text{n}}$ denotes the nullspace projection matrix of Task 1 and $\mathbf{J}_{\text{con}} \in \mathbb{R}^{((6\times\text{n}_\text{s})+(\text{n}_\text{con}-\text{n}_\text{s})\times 3))\times\text{n}}$ is the Jacobian of n_{con} contacts, with n_{s} denoting the number of secondary contacts. $\mathbf{K}_{\text{p}}$ and $\mathbf{K}_{\text{d}}$ are the gain matrices of size $(6 \times \text{n}_{\text{s}}) + (\text{n}_{\text{con}} - \text{n}_{\text{s}}) \times 3$, and $\mathbf{x}_{\text{Perr}}$, $\dot{\mathbf{x}}_{\text{Perr}}$, $\mathbf{x}_{\text{Oerr}}$, and $\dot{\mathbf{x}}_{\text{Oerr}}$ represent the contact pose and velocity errors. The desired motion of the robot is realized with position control, by commanding the reference joint values $\mathbf{q}_{\text{ref}}$, obtained by integrating the reference velocities $\dot{\mathbf{q}}_{\text{ref}}$.

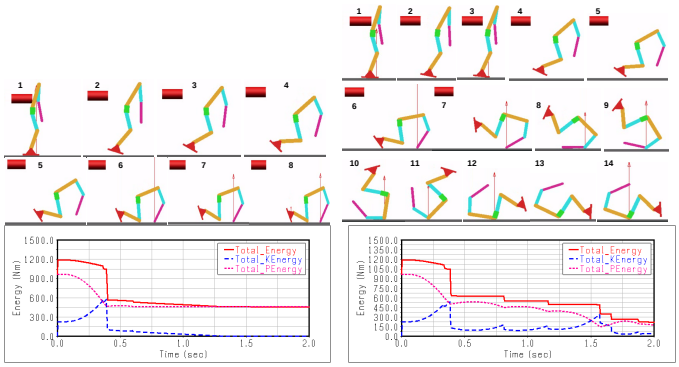

(a) (b)

Fig. 10. Adams simulation results of SPR model (a) without energy injection, (b) with energy injection, where the first row shows the snapshots and the second row shows the potential, kinetic and total energy plots during the course of controlled fall.

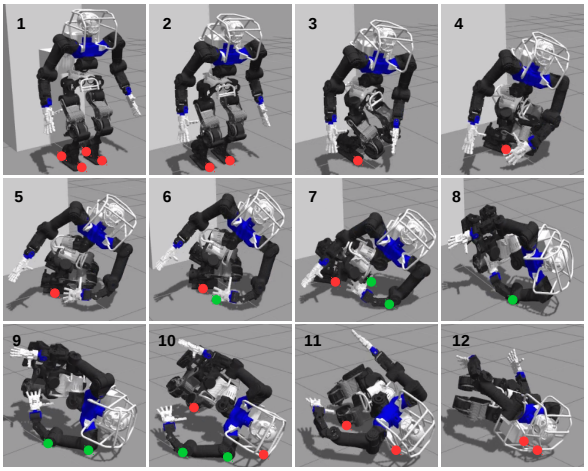

Fig. 11. Simulation snap shots taken during the left side shoulder roll over of the robot with planned (green dots) and unplanned (red contacts) contacts.

VII. Evaluation with SPR Model

In this section, the proposed rolling control scheme is evaluated with the SPR model to analyze the effect of energy injection during controlled fall in detail. An Adams model of the SPR is generated with the specifications of WALK-MAN and the proposed controller in Section VI is applied. The control scheme is implemented as a Matlab-Simulink model to communicate with Adams.

Adams solver settings:- time step: 0.005s; contact model: type (impact), stiffness (1.0E+05 N/mm), force exponent (2.2 no units), damping (10.0 Ns/mm), penetration depth (0.1 mm), friction type (Coulomb), static and dynamic coefficient (0.3 and 0.1 no units), stiction and friction transition velocity (100.0 mm/s and 1000.0 mm/s).

A. With and Without Energy Injection

Figure 10 shows the results of controlled fall simulations obtained with the newly proposed controller. In Fig. 10a, the snapshots at the top and the evolution of energy at the bottom plot denote the results obtained without injecting any additional energy (nEI) into the system, during its fall. Similar results are shown for a controlled fall simulation with an additional injection of energy (wEI) in Fig. 10b. From the snapshots, we can see that the lack of sufficient energy prevents the nEI system from successfully completing its work which involves rolling over the secondary contact (end of lower arm), and hence it is not able to roll over successive contacts as planned. While with wEI, due to the additional injection of energy, the system is able to overcome the *energy drought* condition, as a result, it exhibits successful rolling over the potential contacts as planned, generating a rolling motion. The energy evolution plots also suggest the same with nEI. One major energy dissipation (ΔE = 450 J) is observed during the knee and hand contacts with the ground, following which no significant dissipation is observed. Whereas with wEI, apart from the major energy dissipation (ΔE = 375 J) observed during the lower arm contact with the ground, subsequent energy dissipations due to the elbow (ΔE = 100 J), shoulder (ΔE = 75 J), backpack (ΔE = 150 J), and foot contacts (ΔE = 75 J) are seen, resulting in much higher dissipation of energy (total) and in a gradual manner. This ensures more energy being distributed over multiple contacts, which in turn reduces the impact forces during fall.

VIII. Application to Humanoids

In this section, the proposed online rolling motion generator is applied to the WALK-MAN humanoid model for two reasons. First, to evaluate the effects of applying the proposed controller on a falling over humanoid. Second, to make a quantitative performance comparison between the new fall control scheme and our previously proposed controller. The simulation settings are maintained the same as in [17] to make an effective comparison of the results.

A. Simulation scenarios

Two different scenarios are considered in total to ascertain the effectiveness of the proposed controller as follows: 1) Simulation carried out with our previous controller [17], which is a combination of energy shaping (ES) and energy distribution (ED), and 2) the proposed EIS + RED type control with additional energy injected into the system, which generates a rolling motion. The results are compared between the above two scenarios to evaluate our hypothesis, i.e., rolling over multiple contacts reduces the impact forces significantly. The results are presented and discussed in detail in the following subsections. The backward and side fall results are omitted here due to the page limitations, yet they are included in the video enclosed along with this paper.

B. Energy Comparison

The robot is subjected to a disturbance of 1200 N, applied for 50 ms at 0.9 m height from behind to make it fall over, and the proposed controller is activated upon fall prediction.

In Fig. 11, the snapshots display the robot rolling over its left arm shoulder. Snapshots 2-5 show the humanoid crouching and modifying its left arm pose, resulting in a whole body motion of the humanoid to facilitate it. The crouching action and the forward lunge is due to EIS,

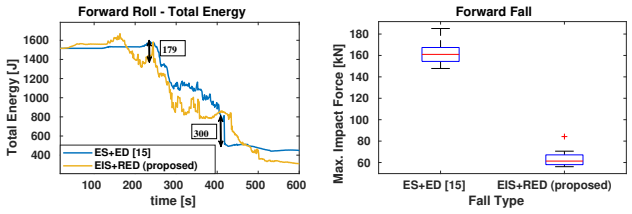

(a) (b)

Fig. 12. Comparison between ES+ED and EIS+RED type falls: (a) Energy dissipation and (b) Statistical plots of the maximum impact force obtained over 10 trials.

and the latter pose modification is because of the control actions generated by RED. In 6, we can observe the final configuration of the left arm, where the hand (E) makes contact with the ground, followed by the wrist and elbow (F) contact in 7, shoulder (G) contact in 9, and finally, in 10-12 the robot rolls over its head and backpack protection frame to its left side making a complete rolling over motion.

Figure 12a compares the evolution of energy between two types of controlled fall actions. Unlike our previous method (ES+ED), we can clearly see three peaks between 300-600 iterations in the total energy plot of EIS+RED, denoting the successive contacts made by the robot and its corresponding dissipation of energy. Relatively, higher instantaneous dissipation of energy (300 J) was observed with ES+ED when compared to that of EIS+RED (179 J), a reduction of 40.3%. The former's high value is due to the static nature of hand contacts, and the latter's low value can be attributed to multiple contacts, its smooth transition resulting in a rolling motion. Also, in roll type control, though e_{v} increases the total kinetic energy due to rollover motion, the number of contacts is increased which in turn reduces the energy dissipated/contact.

C. Impact force comparison

Since the impact force can vary due to the robot's joint compliance, disturbance, simulator (physics engine and contact model), etc., 10 data sets are collected for the humanoid's fall, and the results are compared between different controlled fall actions as shown in Fig. 12b. Overall, we can observe that the impact force (F_{imp}) has been reduced considerably with EIS+RED when compared to the ES+ED type control. With the proposed controller 56.5% of reduction in F_{imp} for the forward fall was observed, compared to ES+ED type control.

IX. Conclusion

We proposed here a rolling motion controller for humanoid fall overs with three major contributions: energy-based control actions; an online rolling controller to compute the critical rolling parameters and energy injection values; and notion of an energy distribution polyhedron to realize the motion. The proposed controller was first evaluated with the SPR model, in particular, to validate the significance of injecting energy (e_{v}) to a falling system. The results showed that with e_{v} it is possible to avoid energy drought and reduce the impact forces considerably by means of rolling. The controller was then applied to a full humanoid, and it is verified that the proposed controller can considerably reduce the impact force by generating rolling motion in comparison to the control without it [17]. The newly proposed one (EIS+RED) exhibited a multi-contact rolling motion, and this reduced the maximum dissipation of energy per contact, which in turn reduced the impact forces significantly.

References

[1] S. Kalyanakrishnan and A. Goswami, "Learning to predict humanoid fall," *International Journal of Humanoid Robotics*, vol. 8, no. 02, pp. 245–273, 2011.

[2] K. Fujiwara *et al.*, "Falling motion control of a humanoid robot trained by virtual supplementary tests." in *Proc. of 2004 IEEE ICRA*, vol. 2, 2004, pp. 1077–1082.

[3] ——, "The first human-size humanoid that can fall over safely and stand-up again," in *Proc. of 2003 IEEE/RSJ IROS*, vol. 2, 2003, pp. 1920–1926.

[4] ——, "Towards an optimal falling motion for a humanoid robot," in *Proc. of 2006 6th IEEE-RAS Humanoids*, 2006, pp. 524–529.

[5] ——, "An optimal planning of falling motions of a humanoid robot," in *Proc. of 2007 IEEE/RSJ Int. Conf. on Intelligent Robots and Systems*, 2007, pp. 456–462.

[6] S.-H. Lee and A. Goswami, "Fall on backpack: Damage minimizing humanoid fall on targeted body segment using momentum control," in *Proc. of 2011 ASME IDETC/CIE*. American Society of Mechanical Engineers, 2011, pp. 703–712.

[7] V. Samy and A. Kheddar, "Falls control using posture reshaping and active compliance," in *Proc. of 2015 IEEE-RAS 15th Humanoids*, 2015, pp. 908–913.

[8] S. Wang and K. Hauser, "Real-time stabilization of a falling humanoid robot using hand contact: An optimal control approach," in *Proc. of 2017 17th IEEE-RAS Humanoids*. IEEE, 2017, pp. 454–460.

[9] Y. Zhou *et al.*, "Falling protective method for humanoid robots using arm compliance to reduce damage," in *Proc. of 2016 IEEE Int. Conf. on Robotics and Biomimetics*, 2016, pp. 2008–2013.

[10] J. Lee *et al.*, "An active compliant impact protection system for humanoids: Application to WALK-MAN hands," in *2016 IEEE-RAS 16th International Conference on Humanoid Robots*. IEEE, 2016, pp. 778–785.

[11] J. Ruiz-del Solar, R. Palma-Amestoy, R. Marchant, I. Parra-Tsunekawa, and P. Zegers, "Learning to fall: Designing low damage fall sequences for humanoid soccer robots," *Robotics and Autonomous Systems*, vol. 57, no. 8, pp. 796–807, 2009.

[12] L. Meng *et al.*, "A falling motion strategy for humanoids based on motion primitives of human falling," in *International Conference on Robotics in Alpe-Adria Danube Region*. Springer, 2017, pp. 264–272.

[13] S.-k. Yun and A. Goswami, "Tripod fall: Concept and experiments of a novel approach to humanoid robot fall damage reduction," in *Proc. of 2014 IEEE ICRA*, 2014, pp. 2799–2805.

[14] S. Ha and C. K. Liu, "Multiple contact planning for minimizing damage of humanoid falls," in *Proc. of 2015 IEEE/RSJ IROS*, 2015, pp. 2761–2767.

[15] D. Luo, Y. Deng, X. Han, and X. Wu, "Biped robot falling motion control with human-inspired active compliance," in *Proc. of 2016 IEEE/RSJ IROS*, 2016, pp. 3860–3865.

[16] V. C. Kumar, S. Ha, and C. K. Liu, "Learning a unified control policy for safe falling," in *2017 IEEE/RSJ Int. Conf. Intelligent Robots and Systems (IROS)*. IEEE, 2017, pp. 3940–3947.

[17] R. Subburaman, J. Lee, D. G. Caldwell, and N. G. Tsagarakis, "Online falling-over control of humanoids exploiting energy shaping and distribution methods," in *2018 IEEE International Conference on Robotics and Automation (ICRA)*. IEEE, 2018, pp. 448–454.

[18] N. G. Tsagarakis, D. G. Caldwell *et al.*, "WALK-MAN: A high-performance humanoid platform for realistic environments," *Journal of Field Robotics*, vol. 34, no. 7, pp. 1225–1259, 2017.

[19] R. L. Jackson, I. Green, and D. B. Marghitu, "Predicting the coefficient of restitution of impacting elastic-perfectly plastic spheres," *Nonlinear Dynamics*, vol. 60, no. 3, pp. 217–229, 2010.

[20] R. Subburaman, J. Lee, D. G. Caldwell, and N. G. Tsagarakis, "Multi-sesnor based fall prediction method for humanoid robots," in *Proc. of 2016 IEEE/RSJ MFI*, 2016, pp. 102–108.